International Journal of Heat and Mass Transfer 198 (2022) 123382

Contents lists available at ScienceDirect

International Journal of Heat and Mass Transfer

journal homepage: www.elsevier.com/locate/hmt

Validation study of a Spatially-Averaged Two-Fluid Model for heat transport in gas-particle flows

Stefanie Rauchenzauner[a,*], Simon Schneiderbauer[a,b]

[a] Christian Doppler Laboratory for Multi-scale Modelling of Multiphase Processes, Johannes Kepler University, Altenbergerstr. 69, Linz, 4040, Austria
[b] Department of Particulate Flow Modelling, Johannes Kepler University, Altenbergerstr. 69, Linz, 4040, Austria

ARTICLE INFO

Article history:
Received 20 April 2022
Revised 19 August 2022
Accepted 21 August 2022
Available online 5 September 2022

Keywords:
Heat transfer
Thermal energy balance
Multiphase turbulence modeling
Multi-scale modeling
Cluster-induced turbulence
Dynamic adjustment

ABSTRACT

We validate a multi-scale turbulence model for the thermal energy estimation in coarse-grid simulations of moderately dense gas-particle flows. The model is based on spatially-averaging the Two-Fluid Model balance equations including the thermal energy balance equation of both phases. We found, that the drift temperature is a valid measure for the heat transfer reduction due to heterogeneous particle clusters. Furthermore, we propose the dynamic estimation of the drift temperature through the application of test-filters and the solution of transport equations for the variances of the phase temperatures and the solid volume fraction. Closure models for the Reynolds stress contributions are based on single-phase Large-Eddy Simulation models, such as gradient assumptions. In this study, we consider different test-cases including Geldart type A and type B particles in moderately dense regimes with domain averaged volume fractions ranging from 0.05 to 0.25. The operating conditions include unbounded sedimentation under gravity, as well as a turbulent-sluggish fluidization. In all cases, we discuss the influence of the meso-scale particle clusters on the macro-scale temperature distributions through the individual contributions of the unresolved terms in coarse-grid simulations. Thereby, we find that the dynamic estimation of the drift temperature leads to accurate results for the influence of local heat sinks on the global temperature difference decay between the phases and that the jump-response of a fluidized bed to an elevated gas-inflow temperature is correctly captured by the proposed multi-phase turbulence model. Furthermore, the importance of the correct estimation of the hydrodynamics for a correct prediction of the thermodynamics is highlighted.

1. Introduction

Reacting gas-particle flows play an active role in well-established and recent advances in chemical engineering and various other industries. Design and optimization of reactors are challenging problems, which need modelling and simulation efforts in order to produce reliable predictions for the operation processes. Since the reacting solid's sizes are usually several orders of magnitude smaller than the reactor dimensions, fully resolved simulations of all scales involved in the process are not feasible, as they are limited by computational power.

A widely used approach is to employ very coarse computational grids to be able to simulate the whole reactor domain in a reasonable time. By doing so, however, information on the unresolved micro- and meso-scale structures is lost. Especially the meso-scale structures, i.e. particle clusters which form due to a clustering instability induced by an external body force, such as gravity, due to the momentum coupling between the phases, were found to have a crucial influence on the macro-scale flow properties. For example, the local and global heat transfer between the phases is considerably overestimated when the effect of cluster-induced turbulence is not accounted for [1].

Many modelling efforts were presented by various groups of researchers to correctly predict the drag-force correction in coarse-grid simulations of gas-particle flows. Since the momentum equations are not the focus of this work, we refer the interested reader to previous studies, i.e. [2–5], and the papers referenced therein. A significantly smaller number has dealt with the influence of the meso-scale structures on the macro-scale heat transfer and temperature distribution [6]. Recently, however, more and more efforts are put in this direction. These advances are equally seen

* Corresponding author at: Christian Doppler Laboratory for Multi-scale Modelling of Multiphase Processes, Johannes Kepler University, Altenbergerstr. 69, Linz, 4040 Austria.
E-mail addresses: stefanie.rauchenzauner@jku.at (S. Rauchenzauner), simon.schneiderbauer@jku.at (S. Schneiderbauer).

https://doi.org/10.1016/j.ijheatmasstransfer.2022.123382

Nomenclature

β	drag coefficient
g	gravitational acceleration
u	solid-phase velocity
v	gas-phase velocity
Δ_f	fine-grid size
γ	interphase heat transfer coefficient
κ_q, q = s,g	effective thermal conductivities of the phases
ν_tq, q = s,g	turbulent viscocities of the phases
ϕ	solid volume fraction
ρ_q, q = s,g	phase densities
Σ_{ik}^fr	frictional stresses
Σ_{ik}^g	gas-phase stresses
Σ_{ik}^kc	kinetic-theory stresses
τ_p	particle response time
τ_T	particle thermal response time
T_g	gas-phase temperature
T_s	solid-phase temperature
ξ_T^*	correlation coefficients
$c_{\mathrm{v,q}}$, q = s,g	specific heat capacities of the phases at constant volume
d_s	particle diameter
k_q, q = s,g	turbulent kinetic energies of the phases
Nu	Nusselt number
p	pressure
Pr_tq, q = s,g	turbulent Prandtl numbers of the phases
Re	particle Reynolds number
Sc_tq, q = s,g	turbulent Schmidt numbers of the phases
T_diff	normalized temperature difference
T_d	drift temperature
SATFM	Spatially-Averaged Two-Fluid Model
TFM	Two-Fluid Model

in the context of pseudo-turbulence, i.e. fluctuations produced by the existence of single particles in the flow. Thereby, information about the unresolved terms on the micro-scale is taken from Particle-Resolved Direct Numerical Simulations (PR-DNS) and closure models for the fluctuating components, such as the pseudo-turbulent heat flux [7], as well as adapted Nusselt number correlations have been proposed [8]. In order to predict the unresolved contributions on the meso-scale, earlier approaches include structure-based energy-minimization multi-scale (EMMS) methods, where Hou and Li [9] developed and validated models for the heat and mass transfer correction due to heterogeneities in gas-particle suspensions. In addition, filtered models, which are derived from spatially-averaging reference Two-Fluid Model (TFM) fine-grid simulation data, were initially derived by Agrawal et al. [10] and subsequently improved by addition of further physical markers [11,12]. In the context of Computational Fluid Dynamics - Discrete Element Models (CFD-DEM), for example, recent studies dealt with the influence of sub-grid heterogeneities on the macro-scale heat transfer and developed filtered models based on CFD-DEM data of mono- [13] and bi-dispersed [14] particle suspensions. A different approach to filtering is the coarse-grained particle model in CFD-DEM. Thereby, a number of particles are treated as one individual larger particle in the simulation in order to reduce the load on computational resources. For the correct estimation of the momentum, heat and mass transfer of the coarse-grained particles, models were developed based on conservation considerations [15,16] or based on the EMMS method in earlier studies [17]. As for the drag correction, newer studies employ machine-learning techniques in order to predict the influence of the meso-scale structures on the heat transfer based on physical markers [18,19]. A multiphase turbulence modelling approach based on Eulerian-Lagrangian simulations of unbounded sedimentation revealed that the covariance between the solid volume fraction and the temperature difference of the phases is the main source of heat transfer reduction in dilute gas-particle flows [20]. This finding can be viewed as an equivalent to the drag-force reduction by the drift velocity, which can be expressed as the covariance between the gas-phase velocity and the solid volume fraction, in rather dilute gas-particle flows [21]. Furthermore, we found in an a priori study, that the drift temperature is also accountable for the heat transfer reduction in moderately dense gas-particle flows [1]. This can directly be related to the drag force reduction due to the drift velocity in moderately dense regimes, which was observed more recently [3,22,23]. Different closure models for the covariance between the volume fraction and the temperature have been proposed, ranging from statistical approaches involving presumed-shape probability distribution functions for the variables [20] to neural-network based predictions for the drift temperature [19]. These approaches rely on the availability of data for the considered cases and it cannot be certain that functional-fit models, presumed-shape probability distribution functions, or neural network weights work well for cases with different parameters than the ones they were initially developed for or trained on. On the other hand, structural models rely on some *a priori* considerations and estimations of the underlying flow-structure. Coarse-grained CFD-DEM models still require more computational power to correctly detect particle collisions and these approaches are often restricted by geometric limitations [24].

In contrast, our new approach is to model the covariance between the solid volume fraction and the gas-phase temperature by the variances of the variables scaled by a linear correlation coefficient. Based on the scale-invariance theory [25], we suggest to calculate the correlation coefficient dynamically in coarse-grid simulations through the application of test-filters known from single-phase LES modelling [26]. Thereby, information on the meso-scale flow properties is locally and dynamically derived from the macro-scale flow variables. Therefore, no specific *a prioi* knowledge about the flow properties is needed, thus, providing a vast applicability in a large variety of cases, including different particle types and operating conditions, as we have shown in the case of a dynamically calculated drift velocity correction to the drag force [2]. Coupled transport equations are solved for the variances of the solid volume fraction, the velocities (i.e. the turbulent kinetic energies) and temperatures of the phases. In this work, we aim to validate the extended approach to scalar transport also in an *a posteriori* analysis. In particular, we aim to validate the drift temperature correction model with the described dynamic adjustment, as well as additional closure models for the unresolved terms in the internal energy balance equations against fine-grid TFM simulation data.

The paper is structured as follows. Firstly, we recall the general idea behind the Spatially-Averaged Two Fluid Model (SATFM) and its applications to the temperature balance equations, including a detailed discussion of the drift temperature closure models and the dynamic adjustment. Furthermore, we describe the test-case set-ups, for which we chose to validate the models, which we derived in an *a priori* study [1], in an *a posteriori* analysis. These include unbounded sedimentation cases, where we observe the influence of the drift temperature on the interphase heat transfer in clustered systems, and a section of an elongated fluidized bed reactor, where we investigate the jump-response to an elevated inflow gas temperature on the overall temperature distribution. Finally, we discuss the simulation results with respect to the impact of each unresolved term on the macro-scale temperature distribution and discuss the validity of the models on differently coarse grid-sizes.

2. The Spatially-Averaged Two-Fluid Model

The SATFM is a multiphase turbulence model aimed at predicting the influence of unresolved meso-scale structures on the macro-scale flow properties. *A priori* investigations of the momentum [3,27] and heat [1] transfer between the gas- and moderately dense solid-phase revealed that, similar to the dilute case [21], drift scalars can be employed to model the effect of clusters, which are not resolved in coarse-grid simulations. As the naming suggests, the models are based on the kinetic-theory Two-Fluid Model equations, which consist of continuous equations of motion for both phases:

$$\frac{\partial \phi}{\partial t} + \frac{\partial}{\partial x_k}(\phi u_k) = 0, \tag{1}$$

$$\frac{\partial (1-\phi)}{\partial t} + \frac{\partial}{\partial x_k}((1-\phi) v_k) = 0, \tag{2}$$

$$\frac{\partial \rho_\mathrm{S} \phi u_i}{\partial t} + \frac{\partial}{\partial x_k}(\rho_\mathrm{S} \phi u_i u_k) = -\phi \frac{\partial p}{\partial x_i} + \frac{\partial}{\partial x_k}\left(\Sigma_{ik}^{\mathrm{kc}} + \Sigma_{ik}^{\mathrm{fr}}\right) + \beta (v_i - u_i) + \phi \rho_\mathrm{S} g_i, \tag{3}$$

$$\frac{\partial \rho_\mathrm{g} (1-\phi) v_i}{\partial t} + \frac{\partial}{\partial x_k}(\rho_\mathrm{g} (1-\phi) v_i v_k) = -(1-\phi)\frac{\partial p}{\partial x_i} + \frac{\partial}{\partial x_k}\Sigma_{ik}^{\mathrm{g}} - \beta (v_i - u_i) + (1-\phi)\rho_\mathrm{g} g_i. \tag{4}$$

Here ϕ represents the solids volume fraction, $\mathbf{u}$ and $\mathbf{v}$ are the solid- and gas-phase velocities, ρ_S and ρ_g are the phase densities, p and Σ_{ik}^{g} are the gas-phase pressure, which is distributed over the phases, and stress tensor, $\mathbf{g}$ is the vector of gravitational acceleration and β is the drag coefficient. In the herein considered moderately dense regimes, drag coefficients proposed, for example, by Wen and Yu [28] or Beetstra et al. [29] can be applied. The microscopic solid-phase stresses $\Sigma_{ik}^{\mathrm{kc}}$ and $\Sigma_{ik}^{\mathrm{fr}}$ are closed by the solving for the granular temperature of the solid phase, a construct similar to the thermodynamic temperature representing the collisions between the particles. Details on the kinetic-theory based TFM can be found in various previous papers, i.e. [30–32], and will not be repeated here. In this work, we will focus on the thermal energy balance equations for both phases:

$$\frac{\partial \phi \rho_\mathrm{s} c_{\mathrm{v,s}} T_\mathrm{s}}{\partial t} + \frac{\partial}{\partial x_k}(\phi \rho_\mathrm{s} c_{\mathrm{v,s}} T_\mathrm{s} u_k) = -\phi p \frac{\partial}{\partial x_k} u_k + \Sigma_{ik}^{\mathrm{kc}} \frac{\partial}{\partial x_k} u_i + \frac{\partial}{\partial x_k}\left(\phi \kappa_\mathrm{s} \frac{\partial}{\partial x_k} T_\mathrm{s}\right) + \gamma (T_\mathrm{g} - T_\mathrm{s}), \tag{5}$$

$$\frac{\partial (1-\phi) \rho_\mathrm{g} c_{\mathrm{v,g}} T_\mathrm{g}}{\partial t} + \frac{\partial}{\partial x_k}((1-\phi) \rho_\mathrm{g} c_{\mathrm{v,g}} T_\mathrm{g} v_k) = -(1-\phi) p \frac{\partial}{\partial x_k} v_k + \Sigma_{ik}^{\mathrm{g}} \frac{\partial}{\partial x_k} v_i + \frac{\partial}{\partial x_k}\left((1-\phi)\kappa_\mathrm{g} \frac{\partial}{\partial x_k} T_\mathrm{g}\right) - \gamma (T_\mathrm{g} - T_\mathrm{s}). \tag{6}$$

Here T_s and T_g are the phase temperatures, $c_{\mathrm{v,g}}$ and $c_{\mathrm{v,s}}$ the specific heat capacities at constant volume, and κ_g and κ_s the effective thermal conductivities of the phases. These balance equations include the transient behaviour, as well as the convection and conduction within the phases. In addition, heat production through viscous heating and the coupling between the kinetic and thermal energy through the compressibility of the phases, the pressure dilatation, is considered. Finally, the interphase heat transfer coefficient is given by:

$$\gamma = \frac{6 \kappa_\mathrm{g} \phi Nu}{d_\mathrm{s}^2}. \tag{7}$$

In this study, we employed the Nusselt number derived by Gunn [33]:

$$Nu = \left(7 - 10 \cdot (1-\phi) + 5 \cdot (1-\phi)^2\right) \cdot \left(1 + 0.7\ Re\ Pr^{1/3}\right) + \left(1.33 - 2.4 \cdot (1-\phi) + 1.2 \cdot (1-\phi)^2\right) \cdot Re^{0.7} Pr^{1/3}.$$

Note that we formulated the temperature equations in terms of the internal energies. Likewise, we can write the balance equations in terms of the enthalpies of the phases using $c_{\mathrm{p,g}}$ and $c_{\mathrm{p,s}}$, the specific heat capacities at constant pressure. Then, also the work of expansion of the phases has to be included in the equations.

Furthermore, we stress that the effective thermal conductivity of the solid phase κ_s is a function of the solid volume fraction and, in particular, of the granular temperature. For further discussion of the individual micro-scale contributions, we refer the interested reader to our previous *a priori* study [1]. We want to highlight, however, that pseudo-turbulence effects, such as the pseudo-turbulent heat flux, are neglected in this study, since the filtered pseudo-turbulent viscosities and thermal conductivities were found to only have insignificant influence on the results of the filtered Two-Fluid Models for sufficiently large filter-sizes [1,3,10,34].

Through the application of spatial filters to the TFM balance Eqs. (1)–(6), we are able to split the variables into their filtered, in other words, resolved part in coarse-grid simulations, and fluctuating components, which need to be modelled. A general description of a spatial filter is given by:

$$\overline{\zeta}(\mathbf{x}, t) = \int_V \omega(\mathbf{x}, \mathbf{y}, \Delta_\mathrm{f})\ \zeta(\mathbf{y}, t)\ \mathrm{d}V_\mathbf{y},$$

with a filter kernel $\omega(\mathbf{x}, \mathbf{y}, \Delta_\mathrm{f})$, which satisfies

$$\int_V \omega(\mathbf{x}, \mathbf{y}, \Delta_\mathrm{f}) \mathrm{d}V_\mathbf{y} = 1,$$

for every point in space $\mathbf{x}$ and every control volume V, whose elongations are larger than the filter size Δ_f. By using Favre-, or phase-averages,

$$\langle T_\mathrm{s} \rangle_\mathrm{S} = \frac{\overline{\phi T_\mathrm{s}}}{\bar{\phi}},$$

$$\langle T_\mathrm{g} \rangle_\mathrm{g} = \frac{\overline{(1-\phi) T_\mathrm{g}}}{(1-\bar{\phi})},$$

we can describe the unresolved components of the variables by:

$$\phi' = \phi - \bar{\phi},$$
$$T_\mathrm{s}'' = T_\mathrm{s} - \langle T_\mathrm{s} \rangle_\mathrm{s},$$
$$T_\mathrm{g}''' = T_\mathrm{g} - \langle T_\mathrm{g} \rangle_\mathrm{g}.$$

We want to emphasize that we use the definition of central moments as proposed by Rauchenzauner and Schneiderbauer [1], Germano [35] for all covariances in this work (especially also the equations in Table 1), since spatial filters do not generally fulfill the identity $\overline{\overline{\zeta}} = \overline{\zeta}$.

In an *a priori* study [1], we employed a budget analysis to conclude which fluctuating components need closure and which can be neglected in comparison to their resolved parts. Thereby, we suggested i.e. to close the Reynolds-stress like contribution, which represents turbulent thermal diffusion, by a gradient assumption closure model, which is widely used in single-phase LES modelling. The turbulent thermal diffusivity was related to the turbulent viscosity by a turbulent Prandtl number of the order of unity. Most importantly, we focused on the interphase heat transfer and found that the resolved heat transfer in coarse-grid simulations severely overestimates the filtered heat transfer and that a sub-grid correction is needed. Therefore, similar to the interphase drag exchange [3], we showed that the resolved heat transfer can be corrected by a drift scalar approach:

$$\overline{\gamma (T_\mathrm{g} - T_\mathrm{s})} \approx \widetilde{\gamma} (\langle T_\mathrm{g} \rangle_\mathrm{g} - \langle T_\mathrm{s} \rangle_\mathrm{s} + T_\mathrm{d}).$$

Here, the drift temperature T_d represents the gas-phase temperature fluctuations *as seen by the particles*, defined as:

$$T_\mathrm{d} = \left\langle T_\mathrm{g}''' \right\rangle_\mathrm{s} := \langle T_\mathrm{g} \rangle_\mathrm{s} - \langle T_\mathrm{g} \rangle_\mathrm{g}.$$

and $\widetilde{\gamma} := \gamma((1-\bar{\phi}), \langle \mathbf{v} \rangle_\mathrm{g}, \langle \mathbf{u} \rangle_\mathrm{s})$ is the microscopic heat transfer coefficient evaluated at the resolved variables. This approximation corresponds to a zeroth order Taylor series expansion of the filtered interphase heat transfer around the resolved variables. Furthermore, we found that the drift velocity can be expressed as a function of the covariance between the solid volume fraction and the gas-phase temperature, therefore, we chose to model T_d by the variances of the variables scaled by a linear correlation coefficient:

$$T_\mathrm{d} \approx \frac{\xi^*_{\mathrm{T}\phi\mathrm{g}} \sqrt{\overline{\phi'^2} \left\langle T_\mathrm{g}''' T_\mathrm{g}''' \right\rangle_\mathrm{g}}}{\bar{\phi}(1-\bar{\phi})}. \tag{8}$$

Here $\left\langle T_\mathrm{g}''' T_\mathrm{g}''' \right\rangle_\mathrm{g}$ is the gas-phase temperature variance, previously referred to as the turbulent internal energy [1]. Transport equations for the variances of the phase temperatures were derived and the unresolved contributions were closed using similar methods to the ones described above [1]. In addition, a transport equation for the variance of the solid volume fraction $\overline{\phi'^2}$ needs to be solved [2].

The corrected linear correlation coefficient is defined as,

$$\xi^*_{\mathrm{T}\phi\mathrm{g}} := \frac{\overline{\phi T_\mathrm{g}} - \overline{\phi}\ \overline{T_\mathrm{g}}}{\sqrt{\overline{\phi'\phi'}} \sqrt{\left\langle T_\mathrm{g}''' T_\mathrm{g}''' \right\rangle_\mathrm{g}}}, \tag{9}$$

and can be calculated locally and dynamically through the application of test-filters in coarse-grid simulations [1–3,23,26].

In the context of finite volume methods, in particular, we apply a second-order approximation of a three-dimensional Gaussian or box filter [2,36–38]:

$$\Omega_{\mathrm{G},2} = 1 + \frac{\Delta_\mathrm{tf}^2}{24} \nabla^2, \tag{10}$$

where ∇^2 is the Laplacian operator and $\Delta_\mathrm{tf} = \sqrt{24/7}\Delta_\mathrm{c}$ is the size of the explicit filter, which is about two times the grid size Δ_c. Therefore, this filter fulfills the requirements for test-filters stated by Germano et al. [39] and coincides with the one used by Parmentier et al. [23].

Therefore, solving the transport equations for the turbulent kinetic energies and the variances of the phase temperatures, as well as a transport equation for the variance of the solids volume fraction combined with the dynamic estimation of the correlation coefficients, allows us to predict the influence of the meso-scale flow structures on the macro-scale hydro- and thermodynamics. Table 1 contains a summary of the fully closed transport equations for the mean internal energies and variances of the phase temperatures [1], which are of particular interest in this study. For a detailed summary of the other transport equations, which are needed to model the hydrodynamics, we refer the reader to our previous study ([2], Table 1). Note that we employ transport equations for the diagonal components of the Reynolds-stress like tensor (the sub-filter stresses) and close the off-diagonal components with correlation coefficients [2,3], thus enabling an anisotropic closure for the (momentum) Reynolds-stress like terms. As stated above, the additional turbulent heat flux is closed nonetheless with a gradient assumption, which we found to be in sufficiently good agreement in an *a priori* analysis [1].

3. Case descriptions

In order to evaluate the different effects of the unresolved contributions in coarse-grid simulations, we set up different test-cases, where we compared the results of fine-grid TFM simulations to the predictions obtained by using the SATFM model. Firstly, we considered unbounded fluidization/sedimentation of Geldart type A particles with different mass loadings. Secondly, we looked at a thin cut-out of an elongated lab-scale fluidized bed reactor of Geldart type B particles. The physical properties of all validation cases are summarized in Table 2.

Concerning the model constants present in the transport equations, we used the ones provided in our previous study [3], where the constants differ sightly between Geldart type A and type B particles. The turbulent Schmidt and Prandtl numbers are set to 1. The enthalpy equation is solved in favor of the internal energy equation, since $c_{\mathrm{p,s}}$ is usually known.

The simulations were conducted using the open-source CFD software OpenFOAM 6 (http://www.openfoam.org), where we modified the two-phase flow solver `twoPhaseEulerFoam` to incorporate the SATFM turbulence models. The modified solver can be downloaded via github at https://github.com/ParticulateFlow/pfmFOAM-public.git. The pressure-velocity coupling was solved using the PIMPLE algorithm. We used the Gaussian theorem together with linear interpolation to discretize the diffusive terms in the balance equations, whereas the SuperBee flux-limiter was used for the extrapolation of the convective terms [2,40], since flux-limiters were shown to yield good predictions for bubble-shapes in previous studies [41,42]. Furthermore, we used first-order implicit schemes for time advancement, which are bounded.

For the dynamic adjustment, we employed Eq. (10) with $\Delta_\mathrm{tf} = \sqrt{24/7}\Delta_\mathrm{c}$, using the Laplacian operator implemented in OpenFOAM. Similar to single-phase LES modelling, we observed that the dynamic procedure can produce results with large fluctua-

Table 1
Transport equations for the mean internal energies and variances of the phase temperatures [1].

SA-TFM balance equation for the internal energy of the solid- and gas phase:

$$\frac{\partial \bar{\phi}\langle T_\mathrm{s}\rangle_\mathrm{s}}{\partial t} + \frac{\partial}{\partial x_k}\left(\bar{\phi}\langle T_\mathrm{s}\rangle_\mathrm{s}\langle u_k\rangle_\mathrm{s}\right) = \frac{1}{c_{\mathrm{v,s}}\rho_\mathrm{s}}\left[\frac{\partial}{\partial x_k}\left(\bar{\phi}\langle\kappa_\mathrm{s}\rangle_\mathrm{s}\frac{\partial}{\partial x_k}\langle T_\mathrm{s}\rangle_\mathrm{s}\right) + \widetilde{\gamma}\left(\langle T_\mathrm{g}\rangle_\mathrm{g} - \langle T_\mathrm{s}\rangle_\mathrm{s} + T_\mathrm{d}\right) - \bar{\phi}\ \overline{p}\frac{\partial}{\partial x_k}\langle u_k\rangle_\mathrm{s} + \overline{\Sigma^{\mathrm{kc}}_{ik}}\frac{\partial}{\partial x_k}\langle u_i\rangle_\mathrm{s} + C_\epsilon \bar{\phi} k_\mathrm{s}\sqrt{\widetilde{S}^{\mathrm{s}}_{ij}\widetilde{S}^{\mathrm{s}}_{ij}}\right] + \frac{\partial}{\partial x_k}\left(\bar{\phi}\frac{\nu_{\mathrm{ts}}}{Pr_{\mathrm{ts}}}\frac{\partial}{\partial x_k}\langle T_\mathrm{s}\rangle_\mathrm{s}\right). \tag{11}$$

$$\frac{\partial (1-\bar{\phi})\langle T_\mathrm{g}\rangle_\mathrm{g}}{\partial t} + \frac{\partial}{\partial x_k}\left((1-\bar{\phi})\langle T_\mathrm{g}\rangle_\mathrm{g}\langle v_k\rangle_\mathrm{g}\right) = \frac{1}{c_{\mathrm{v,g}}\rho_\mathrm{g}}\left[\frac{\partial}{\partial x_k}\left((1-\bar{\phi})\kappa_\mathrm{g}\frac{\partial}{\partial x_k}\langle T_\mathrm{g}\rangle_\mathrm{g}\right) - \widetilde{\gamma}\left(\langle T_\mathrm{g}\rangle_\mathrm{g} - \langle T_\mathrm{s}\rangle_\mathrm{s} + T_\mathrm{d}\right) - (1-\bar{\phi})\overline{p}\frac{\partial}{\partial x_k}\langle v_k\rangle_\mathrm{g} + \overline{\Sigma^{\mathrm{g}}_{ik}}\frac{\partial}{\partial x_k}\langle v_i\rangle_\mathrm{g} + C_\epsilon \mathrm{g}(1-\bar{\phi})k_\mathrm{g}\sqrt{\widetilde{S}^{\mathrm{g}}_{ij}\widetilde{S}^{\mathrm{g}}_{ij}}\right]$$
$$+ \frac{\partial}{\partial x_k}\left((1-\bar{\phi})\frac{\nu_{\mathrm{tg}}}{Pr_{\mathrm{tg}}}\frac{\partial}{\partial x_k}\langle T_\mathrm{g}\rangle\mathrm{g}\right). \tag{12}$$

Transport equation for the variance of the solid-phase temperature:

$$\frac{\partial \bar{\phi}\left\langle T_\mathrm{s}'' T_\mathrm{s}''\right\rangle_\mathrm{s}}{\partial t} + \frac{\partial}{\partial x_k}\left(\bar{\phi}\langle T_\mathrm{s}'' T_\mathrm{s}''\rangle_\mathrm{s}\langle u_k\rangle_\mathrm{s}\right) = \frac{\partial}{\partial x_k}\left(\bar{\phi}\frac{\nu_{\mathrm{ts}}}{Sc_{\mathrm{ts}}}\frac{\partial}{\partial x_k}\langle T_\mathrm{s}'' T_\mathrm{s}''\rangle_\mathrm{s}\right) + 2\bar{\phi}\frac{\nu_{\mathrm{ts}}}{Pr_{\mathrm{ts}}}\frac{\partial}{\partial x_k}\langle T_\mathrm{s}\rangle_\mathrm{s}\frac{\partial}{\partial x_k}\langle T_\mathrm{s}\rangle_\mathrm{s} + \frac{2}{c_{\mathrm{v,s}}\rho_\mathrm{s}}\left[-C_{\mathrm{ds}}\sqrt{\langle T_\mathrm{s}'' T_\mathrm{s}''\rangle_\mathrm{s}}\bar{\phi}\ \overline{p}\frac{\partial}{\partial x_k}\langle u_k\rangle_\mathrm{s} + \widetilde{\gamma}\left(\xi^*_{\mathrm{Tgs}}\sqrt{\langle T_\mathrm{s}'' T_\mathrm{s}''\rangle_\mathrm{s}\left\langle T_\mathrm{g}''' T_\mathrm{g}'''\right\rangle_\mathrm{g}} - \langle T_\mathrm{s}'' T_\mathrm{s}''\rangle_\mathrm{s}\right)\right]. \tag{13}$$

Transport equation for the variance of the gas-phase temperature:

$$\frac{\partial (1-\bar{\phi})\left\langle T_\mathrm{g}''' T_\mathrm{g}'''\right\rangle_\mathrm{g}}{\partial t} + \frac{\partial}{\partial x_k}\left((1-\bar{\phi})\left\langle T_\mathrm{g}''' T_\mathrm{g}'''\right\rangle_\mathrm{g}\langle v_k\rangle_\mathrm{g}\right) = \frac{\partial}{\partial x_k}\left((1-\bar{\phi})\frac{\nu_{\mathrm{tg}}}{Sc_{\mathrm{tg}}}\frac{\partial}{\partial x_k}\left\langle T_\mathrm{g}''' T_\mathrm{g}'''\right\rangle_\mathrm{g}\right) + 2(1-\bar{\phi})\frac{\nu_{\mathrm{tg}}}{Pr_{\mathrm{tg}}}\frac{\partial}{\partial x_k}\langle T_\mathrm{g}\rangle\mathrm{g}\frac{\partial}{\partial x_k}\langle T_\mathrm{g}\rangle\mathrm{g} + \frac{2}{c_{\mathrm{v,g}}\rho\mathrm{g}}\left[-C_{\mathrm{dg}}\sqrt{\left\langle T_\mathrm{g}''' T_\mathrm{g}'''\right\rangle_\mathrm{g}}(1-\bar{\phi})\overline{p}\frac{\partial}{\partial x_k}\langle v_k\rangle_\mathrm{g}\right.$$
$$\left. + \widetilde{\gamma}\left(\xi^*_{\mathrm{Tgs}}\sqrt{\langle T_\mathrm{s}'' T_\mathrm{s}''\rangle_\mathrm{s}\left\langle T_\mathrm{g}''' T_\mathrm{g}'''\right\rangle_\mathrm{g}} - \xi_{\mathrm{Tg@s}}\left\langle T_\mathrm{g}''' T_\mathrm{g}'''\right\rangle_\mathrm{g} - \xi^*_{\mathrm{T}\phi\mathrm{g}}\frac{\sqrt{\overline{\phi'^2}\left\langle T_\mathrm{g}''' T_\mathrm{g}'''\right\rangle_\mathrm{g}}}{\bar{\phi}(1-\bar{\phi})}\left(\langle T_\mathrm{g}\rangle\mathrm{g} - \langle T_\mathrm{s}\rangle\mathrm{s}\right)\right)\right]. \tag{14}$$

Table 2
Physical properties of the different validation cases. Here ϕ^{max} denotes the maximum packing limit and ϕ^{fr} is the minimum solid volume fraction at which the long-lasting contacts between particles are considered dominant and the frictional viscosity is calculated. The particle Froude number is defined as $Fr_p = u_t/(gd_s)$, where u_t denotes the terminal settling velocity and g the standard acceleration due to gravity. The operator $\langle\rangle_d$ represents the average over the whole domain. The fine-grid size is represented by Δ_f, while the coarse-grid sizes considered are given as Δ_c.

property	unbounded fluidzation Fullmer (2016)	dilute unbounded fludization Guo (2019)	fluidized bed
ϕ^{max}	0.64	0.6	0.6
fric. model	Schaeffer [43]	Schneiderbauer et al. [44]	
ϕ^{fr}	0.6	0.4	0.4
$\rho_g/(kg/m^3)$		1.224	
$\mu_g/(kg/m\ s)$		$1.8 \cdot 10^{-5}$	
$\rho_s/(kg/m^3)$	1500	1300	2500
drag model		Beetstra et al. [29]	Wen and Yu [28]
$\kappa_g/(W/m\ K)$		$2.4 \cdot 10^{-2}$	
$c_{v,g}/(J/kg\ K)$		718	
$c_{p,g}/(J/kg\ K)$		1007	
$c_{p,s}/(J/kg\ K)$		1000	750
d_s/m	$75 \cdot 10^{-6}$	$90 \cdot 10^{-6}$	$150 \cdot 10^{-6}$
$u_t/(m/s)$	0.22	0.26	0.96
Fr_p	65	76	626
$\langle\phi\rangle_d$	0.05, 0.15, 0.25	0.05	0.2
Δ_f/d_s	3	2	7
Δ_c/d_s	24	32,64	35,63

tions. Therefore, we limit the coefficients by their theoretical limits [1,2] and smooth the results using an additional spatial filter, namely,

$$\overline{\xi}(x,t) = \frac{\sum_{faces} A_f(x,t)\xi_f(x,t)}{\sum_{faces} A_f(x,t)},$$

where A_f is the area of the faces and ξ_f is the value of the variable at the faces. This represents a weighted average in terms of the cell-center values, for which the weight of the center cell is slightly higher than those of the surrounding cells.

3.1. Unbounded fluidization

In order to provide some comparability, we focused on two test-cases, which were previously discussed in literature. Firstly, the slightly smaller test-case set-up of Fullmer and Hrenya [40], which was investigated with CFD-DEM also by Radl and Sundaresan [45] is evaluated for different domain averaged solid volume fractions. Previous literature only focused on the isothermal description of this test-case, in particular on the correct estimation of the slip-velocity. We will consider heat transfer in this environment. Secondly, we examine a case with domain averaged solids volume fraction of 0.05 based on the work of Guo and Capecelatro [20], where the heat transfer in rather dilute regimes was investigated through Eulerian-Lagrangian simulations.

In all of the unbounded sedimentation cases we started the simulations from a slightly non-uniform distribution of isothermal particles in air inside a computational domain, where we applied periodic boundary conditions in every direction. Due to gravity, the particles start to settle and clusters of particles form due to the momentum coupling between the two phases. Note that we assume that the fluid pressure can be decomposed into a fluctuating (local) component superimposed by a linear gradient, where the latter opposes gravity and supports the weight of the suspension, i.e. [2,46,47],

$$\nabla p = \left(\langle\phi\rangle_d \rho_s + (1 - \langle\phi\rangle_d)\rho_g\right)\boldsymbol{g}.$$

Here, $\langle\cdot\rangle_d$ denotes the domain average and $\boldsymbol{g}$ is the vector of gravitational acceleration. Starting from an initial transient settling behaviour, the system finally reaches a statistically steady-state with persistent temporarily and spatially distributed clusters. After the fully developed CIT is ensured at about $t \approx 100\tau_p - 120\tau_p$ [20], where we estimate the particle response time by $\tau_p := u_t/g$, the effect of the meso-scale heterogeneities on the heat transfer is investigated.

This particular set-up is used to isolate the influence of the drift temperature correction on the overall temperature balance in the domain. Therefore, the gas-phase temperature is set to 500 K uniformly in the whole domain, while the solid-phase temperature is kept at 300 K. Note that we keep the gas-phase density constant in our simulations since the expansion of the gas can not realistically be captured by the periodic box set-up, which ensures constant mass inside the domain. Furthermore, the gas temperature assimilates very fast to the solids', such that we neglect the change in gas-phase density. In order to estimate the general heat transfer inside the whole domain, we consider the normalized temperature difference between the phases [20],

$$T_{diff} := \frac{T_g - T_s}{T_{0,g} - T_s}, \tag{15}$$

where $T_{0,g} = 500$ K is the gas-phase temperature at the time at which heat transfer is enabled, t_0.

Note that, in the unbounded sedimentation cases, we had to limit the timestep in the simulations to 10^{-7} s to ensure a stable solution process, since instantaneously setting the temperature difference in the whole domain to 200 K lead to a very high heat transfer between the phases, which happened significantly faster than the momentum transfer. This will be further discussed in the results and discussion Section 4.1.

In the first set-up, we investigated Geldart type A particles with different domain averaged volume solids fractions of $\langle\phi\rangle_d = 0.05, 0.15, 0.25$. The domain size was $32 \times 32 \times 128$ grid cells for the fine-grid simulations, allowing us to consider coarse-graining ratios of up to $\Delta_c/\Delta_f = 8$. The geometry is despicted in Fig. 1 a). The predicted values for the mean-slip Reynolds numbers, $Re_{slip} := \rho_g d_s \langle u_{slip}\rangle_d/\mu_g$, calculated from the domain averaged slip velocity in vertical z-direction in the domain,

$$\langle u_{slip}\rangle_d = \frac{\langle(1-\bar{\phi})\langle v_z\rangle_g\rangle_d}{1 - \langle\bar{\phi}\rangle_d} - \frac{\langle\bar{\phi}\langle u_z\rangle_s\rangle_d}{\langle\bar{\phi}\rangle_d}, \tag{16}$$

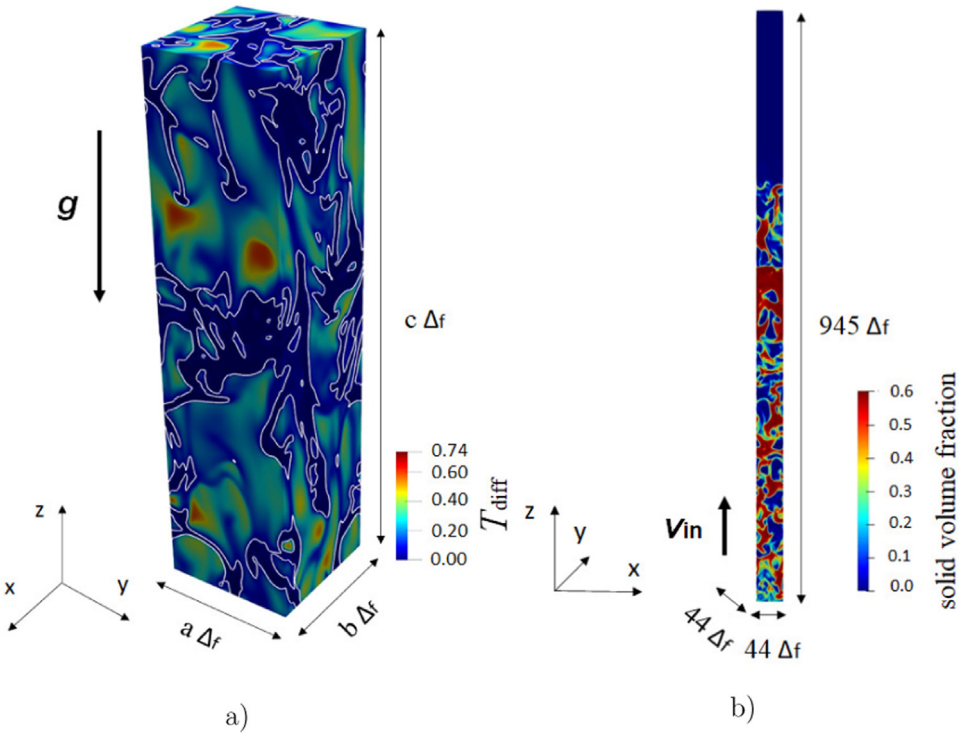

Fig. 1. Test case geometries. a) Periodic box setup with $a \times b \times c = 32 \times 32 \times 128$, and $a \times b \times c = 128 \times 128 \times 512$, respectively. The snapshot shows the normalized temperature difference between the phases at $t = t_0 + 0.004\tau_p$, together with the isosurfaces of the domain averaged solid volume fraction of 0.05 depicted as white lines. b) Fluidized bed dimensions and volume fraction distribution at $t = 4$ s.

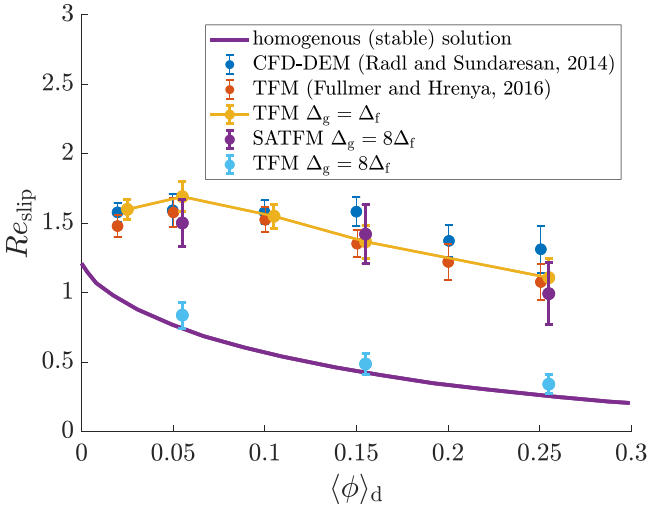

Fig. 2. Mean-slip Reynolds number Re_{slip} for different domain averaged solid volume fractions $\langle\phi\rangle_d$ in the case of moderately dense unbounded sedimentation with $u_t = 0.22$ m/s, including a comparison with the reported values of other TFM [40] and CFD-DEM [45] simulations in literature.

are visualized in Fig. 2, for the fine-grid TFM, coarse-grid TFM and SATFM simulations. As can be deduced from Fig. 2, the fine-grid TFM simulation values are in good agreement with the TFM results of Fullmer and Hrenya [40], where we used the same drag correlation, and slightly deviant from the CFD-DEM results obtained by Radl and Sundaresan [45], since the slip velocity is underestimated for larger solid volume fraction loadings. Furthermore, we want to note that, although the flow is in a statistically steady state, the instantaneous slip velocity values fluctuate around its mean due to the breaking and forming of clusters. Due to the model corrections, the fluctuations are larger for the SATFM simulations, leading to larger error bars in the determination of the mean slip velocity. All in all, however, the SATFM produces good results for the slip velocity for all considered solids mass loadings.

In addition to the relatively smaller periodic box set-up described before, we considered a similar case to the ones treated in [20], where domain averaged volume fractions up to 0.05 were investigated. Note that we used the same drag correlation as for the smaller periodic box, namely the Beetrsta et al. [29] drag coefficient, while Guo and Capecelatro [20] used an adapted Stokes drag law for their considered mostly dilute cases. Here a grid with $128 \times 128 \times 512$ cells was used for the fine-grid TFM simulations. The larger dimensions provide us with the opportunity to use larger coarse-graining ratios. Although, we found that the kinetic-theory based Two-Fluid Model yields good results for both, the momentum and heat transfer for a coarse graining factor of up to $\Delta_c/\Delta_f = 5$, which is in accordance to the findings of Fullmer and Hrenya [40], who stated that coarser grids can be used for TFM simulations of Geldart type A particles if the flow is more dilute, i.e. if the domain-averaged solid volume fraction is lower.

3.2. Fluidized bed cut-out

Finally, we consider a thin cut-out of an elongated lab-scale fluidized bed reactor of Geldart type B particles without the influence of wall-effects. Therefore, we employ periodic boundary conditions in the lateral directions in the simulations. Note that the applicability and validity of the test-filtering approach in the vicinity of walls was already shown in our previous study [2]. The physical properties are given in Table 2. The superficial gas velocity at the bottom inlet is set to 0.63 m/s and a freeboard is considered on the top of the fluidized bed. The time-step employed in the simulations was variable but limited to ensure that the maximum Courant number did not exceed the value of 0.25, which was around 10^{-4} s.

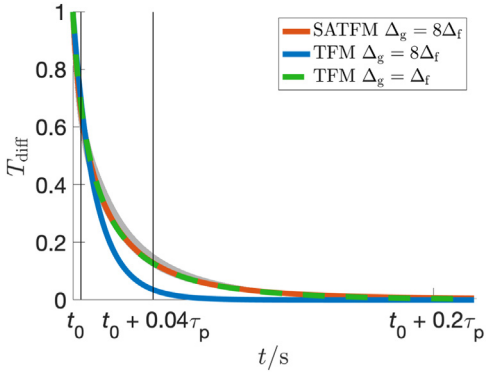

Fig. 3. Normalized temperature difference decay predicted by TFM simulations on a fine grid with $\Delta_g = \Delta_f$ and on a coarse grid with $\Delta_g = 8\Delta_f$, compared to the predictions of the SATFM on a coarse grid with $\Delta_g = 8\Delta_f$, for a domain averaged solid volume fraction of 0.15. The light gray shaded region represents the standard deviation around the mean value of 5 SATFM simulations on the coarse grid with $\Delta_g = 8\Delta_f$, where we used different initial conditions, i.e. different t_0, for each simulation.

In particular, we want to investigate a step-response of the gas- and particle-phase temperatures in the fluidized bed reactor. The simulations were started from a slightly non-homogeneous settled state with isothermal conditions, where $T_s = T_g = 300$ K. Heat transfer between the phases, as well as heat generation through viscous dissipation and pressure dilatation was enabled from the start through the solution of the enthalpy balance equations, which are equivalent to equations (11) and (12). After the initial transient bed expansion, at $t_0 = 3\ \text{s} \approx 30\tau_p$, the inlet air temperature was changed from the initial value of 300 K to 800 K. At $t = 4$ s, the gas-phase inlet temperature was again decreased to 300 K. In order to quantify the step-response of the fluidized bed to this jump in inlet temperature, we investigated the temperature distributions inside the fluidized bed at time $t = 5$ s, where temperature differences had started to evened out over the entire height of the fluidized bed.

4. Results and discussion

4.1. Unbounded fluidization

Figure 3 depicts the decay of the normalized temperature difference between the phases T_{diff}, Eq. (15), for a domain-averaged solids volume fraction of 0.15. As can be seen in the figure, the predictions of the TFM without any sub-grid corrections on the coarse grid, with $\Delta_g/\Delta_f = 8$, yield a faster decay of the temperature difference between the phases, since it does not take the heterogeneity of the flow into account. The predictions of the SATFM on the same coarse grid, however, are in excellent agreement with the fine-grid TFM simulation. It has to be noted that, the heat transfer between the phases happens in under $0.2\tau_p$, further underlining the fact that the particle thermal response time, which is inversely proportional to the heat transfer coefficient [48], is much smaller than the particle (momentum) response time. In the following, we will identify the particle thermal response time τ_T as the time after which the global temperature difference becomes 36.8% or $1/e$ of its initial value [48]. Furthermore, Fig. 4 shows the predicted instantaneous filtered heat transfer as a function of the solid volume fraction for different instances of time, a) at $t = t_0 + 0.004\tau_p$ and b) at $t_0 = t + 0.04\tau_p$. Initially, the filtered heat transfer predicted by the coarse-grid TFM simulation is too high, which is in accordance to previous studies [1]. After this initial phase, however, the predicted temperature difference is already much lower than the one predicted by the fine-grid TFM simulation, therefore, at $t_0 = t + 0.04\tau_p$, the instantaneous heat transfer predicted by the coarse-grid simulation is already lower than the predictions of the fine-grid simulation, as can be seen in Fig. 4 b). Overall, this leads to an overestimated decay of the global temperature difference between the phases T_{diff}. Concerning the sub-grid statistics, such as the variance of the gas-phase temperature $\langle T_g''' T_g''' \rangle_g$, and especially the drift temperature, we evaluated them from the coarse-grid and fine-grid simulations and binned the values with respect to the solid volume fraction. Note that, on the one hand, the solid volume fraction range is smaller in the coarse-grid simulations due to the averaging nature of the coarse grid, and on the other hand, the instantaneous coarse-grid simulation data shows higher fluctuations due to much lesser available data for the individual volume fraction bins. Here, we depicted the variance of the gas-phase temperature $\langle T_g''' T_g''' \rangle_g$ as a function of the solid volume fraction, for which we solve a transport equation and which, according to Eq. (8), needs to be estimated for the prediction of the drift temperature together with the variance of the solids volume fraction and the correlation coefficient between the solid volume fraction and the gas-phase temperature (9). It can be deduced from Fig. 4 that the transport equation yields satisfying estimates for the variance of the gas-phase temperature in the coarse-grid simulations, while it is overestimated initially, but the dependence on the solids volume fraction is correctly captured. Furthermore, the dynamic adjustment of the correlation coefficient leads to good predictions for the shape and size of the drift temperature. Due to the decay in gas-phase temperature, variance of the gas-phase temperature and the drift temperature decay with time as well.

Since the physical quantities, especially the slip velocity, fluctuate around a statistical mean value during the course of the simulations, we tested the robustness of the SATFM model by using different starting configurations and initial conditions for the heat transfer simulations. This was realized by choosing different timesteps from the cold sedimentation case as our t_0. The light gray shaded region in Fig. 3 represents the standard deviation around a mean of the predictions of 5 different SATFM simulations on the coarse grid. The 5 initial conditions were chosen in the range of approximately $10\tau_p$. We observe that the predictions vary slightly, however, we can conclude that the overall temperature decay is robustly predicted for all considered initial conditions.

Finally, we also evaluated the global temperature difference decay for domain-averaged solids volume fractions of 0.05 and 0.25. As can be observed from Fig. 5, SATFM simulations with the same set-up and parameters will produce accurate results for all considered volume fractions, ranging from rather dilute to moderately dense. Furthermore, it can be observed that the normalized temperature decay happens faster in higher mass loading regimes. The fine-grid temperature decay curves for the 0.15 and 0.25 solid volume fraction cases, however, are very similar with $\tau_T|_{\langle\phi\rangle_d=0.15} = 0.0003\ \text{s} \approx 0.013\tau_p$ and $\tau_T|_{\langle\phi\rangle_d=0.25} = 0.0002\ \text{s} \approx 0.009\tau_p$. Additionally, both curves reach the threshold of $T_{diff} \leq 10^{-2}$ at $t = t_0 + 0.16\tau_p$ and $t = t_0 + 0.17\tau_p$, respectively. There is only a slight difference in the slope at intermediate times around $t = t_0 + 0.03\tau_p$. While the 0.05 volume fraction case has a thermal response time of $\tau_T|_{\langle\phi\rangle_d=0.05} = 0.0011\ \text{s} \approx 0.05\tau_p$ and reaches the threshold only after $0.3\tau_p$, showing the different influence of clusters on the heat transfer depending on the domain averaged solids volume fraction.

In the relatively larger domain with 90 μm particles, we can investigate coarse graining ratios of up to $\Delta_g/\Delta_f = 32$, that corresponds to 4 grid cells in the lateral directions, same as for the coarse simulations in the smaller domain. In Fig. 1, a snapshot of the normalized temperature difference distribution after at $t = t_0 + 0.004\tau_p$ is shown, together with the isosurfaces of the domain averaged solid volume fraction of 0.05, further indicating that dif-

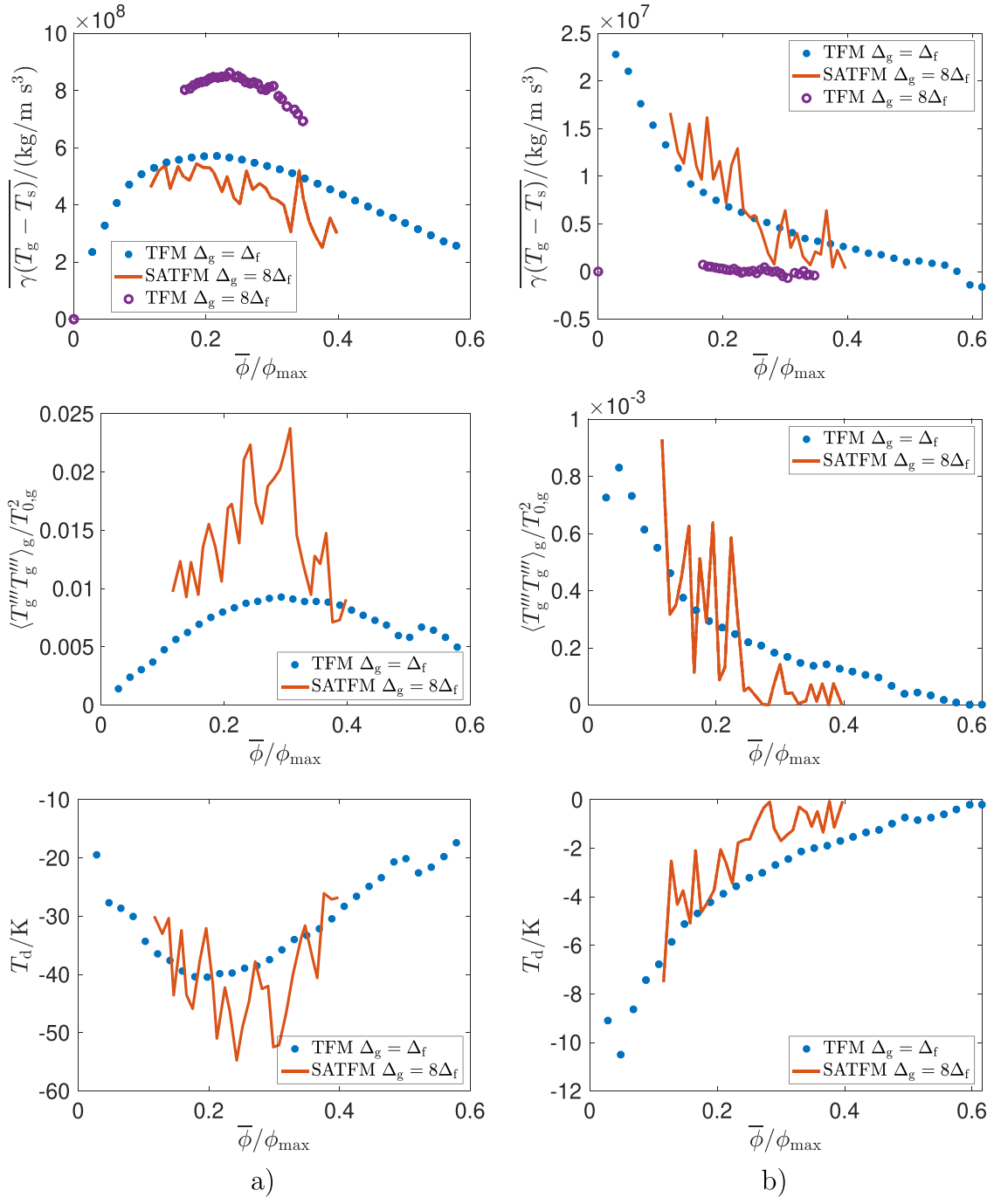

Fig. 4. Filtered temperature transfer $\overline{\gamma(T_g - T_s)}$, variance of the gas-phase temperature $\langle T_g''' T_g''' \rangle_g$, and drift temperature T_d calculated from the fine-grid TFM simulation data with $\Delta_g = \Delta_f$ and predicted by the SATFM model on a coarse grid with $\Delta_g = 8\Delta_f$ at different instances of time; a) at $t = t_0 + 0.004\tau_p$, and b) at $t = t_0 + 0.04\tau_p$, in the case of unbounded sedimentation with a domain-averaged solid volume fraction of 0.15. The prediction for the filtered temperature transfer by an uncorrected TFM simulation on a coarse numerical grid with $\Delta_g = 8\Delta_f$ is also depicted.

ferences of temperature prevail only in regions, which are devoid of clusters. As can be deduced from Fig. 6, the SATFM model yields similar results for different considered coarse-graining ratios of 16 and 32. The particle thermal response time is $\tau_T \approx 0.055\tau_p$, which is slightly larger than in the smaller domain with 75 μm particles, while the threshold of $T_{diff} \leq 10^{-2}$ is reached at $t = t_0 + 0.4\tau_p$. In the paper of Guo and Capecelatro [20], a similar figure shows the temperature difference decay for a domain averaged solid volume fraction of 0.01. In the 0.01 volume fraction case, the thermal particle response time is $\tau_T \approx 0.12\tau_p$, and the threshold is reached at $t = t_0 + 0.97\tau_p$, which further shows the naturally slower temperature difference decay for lower mass loading cases.

As was already mentioned in Section 3.1, the uncorrected TFM yields valid results for the momentum and heat transfer for coarse-graining ratios of up to $\Delta_g/\Delta_f = 5$. Due to the averaging nature of the SATFM and the assumptions made in the derivation process [1], which are only valid for larger coarse-graining ratios, where e.g. the granular temperature can be neglected in comparison to the meso-scale Reynolds-stress, the SATFM does not yield the same results for coarse-graining ratios of up to $\Delta_g/\Delta_f = 5$.

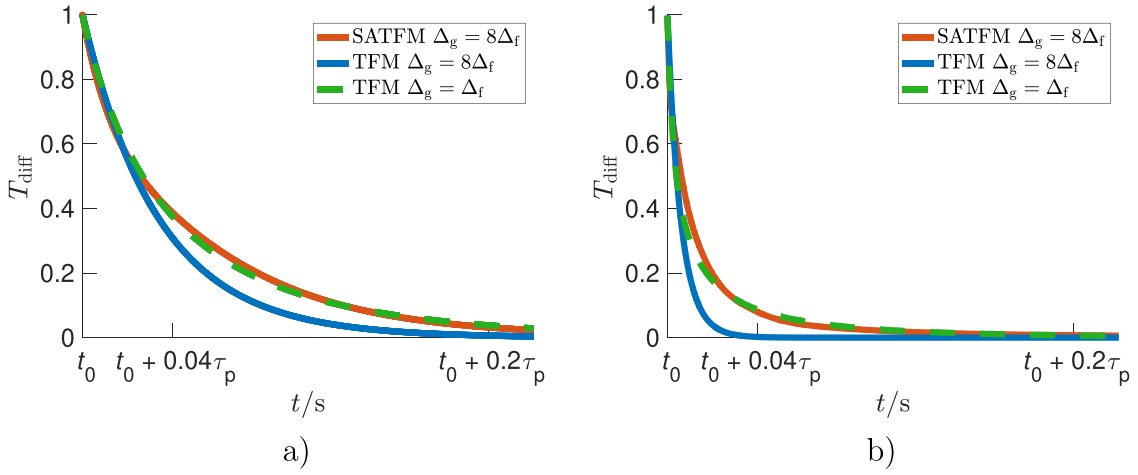

Fig. 5. Normalized temperature difference decay predicted by TFM simulations on a fine grid with $\Delta_g = \Delta_f$, and on a coarse grid with $\Delta_g = 8\Delta_f$ compared to the predictions of the SATFM on a coarse grid with $\Delta_g = 8\Delta_f$ for a domain averaged solid volume fraction of a) 0.05 and b) 0.25.

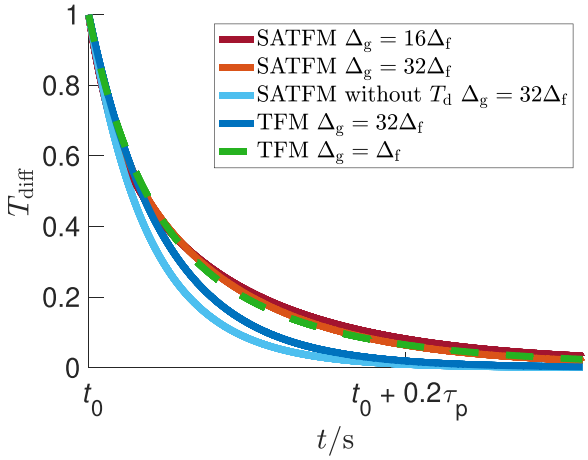

Fig. 6. Normalized temperature difference decay predicted by TFM simulations on a fine grid with $\Delta_g = \Delta_f$, and on a coarse grid with $\Delta_g = 32\Delta_f$ compared to the predictions of the SATFM on differently coarse grids in the dilute sedimentation case with $\langle\overline{\phi}\rangle_d = 0.05$. For a grid with size $\Delta_g = 32\Delta_f$, a comparison between the SATFM model and the SATFM without a drift temperature correction is shown.

Finally, since the unbounded sedimentation test-cases were designed to isolate the influence of the interphasial heat transfer on the thermal energy balance equations of the phases alone, we also wanted to investigate how the predictions differ if we do not apply the drift temperature correction to the interphase heat exchange term. Thereby, we used the SATFM for the momentum and heat equations but set the drift temperature value to zero everywhere. The result can be seen in Fig. 6 for $\Delta_g/\Delta_f = 32$. In comparison to the SATFM with a drift temperature correction, the decay of the temperature difference is overestimated, as can be expected, however, the temperature difference decay is even overestimated in comparison to the coarse-grid TFM simulation results. This is due to the fact that the interphase heat exchange coefficient (7) is a function of the particle Reynolds number and, therefore, of the slip velocity. Since the slip velocity is underestimated in coarse-grid simulations but correctly estimated in SATFM simulations, the value of the heat transfer coefficient is much higher in the SATFM simulations, therefore, leading to even larger errors if only the hydrodynamic is corrected, but no drift temperature correction is applied to the already overestimated interphase heat exchange. This could lead to the conclusion that correcting the hydrodynamics but not the thermodynamics leads to worse predictions than applying no sub-grid correction models at all. However, in this specific set-up, we keep the domain averaged volume fraction constant, as was explained in Section 3.1. This is usually not the case in reactors, since an overestimation of the gas-particle drag force leads to considerably wrong predictions for the solid volume fraction distributions, like an overestimated bed expansion in fluidized bed reactors. However, as will be explained in the following Section 4.2, the correct estimation of the solid volume fraction distribution is crucial for the correct prediction of the overall heat transfer in turbulent bubbling fluidized beds.

4.2. Fluidized bed cut-out

In contrast to the unbounded sedimentation set-up, the dominant unresolved contributions in the fluidized bed set-up include the turbulent temperature diffusion in addition to the heat transfer correction. Furthermore, the influence of the correct estimation of the hydrodynamics on the thermodynamics can be observed. In the periodic-box set-up, we wanted to investigate a case, where only the drift temperature contribution to the whole heat distribution inside the domain would be visible, similar to Guo and Capecelatro [20]. Thereby, we kept the domain-averaged volume fraction constant through the application of a stabilizing pressure gradient as explained in Section 3.1. This lead to the conclusion, that correcting only the momentum, but not the heat transfer in coarse-grid simulations yields worse results for the estimation of the temperatures in the domain than coarse-grid simulations with no corrections, as can be seen in Fig. 6. However, in a realistic set-up of a fluidized bed, we observe that this does not hold true and that it is important to have a correct estimation of the hydrodynamics. While in the coarse-grid TFM simulation, the bed expansion is considerably overestimated, as can be seen in Fig. 7, the temperature distribution inside the fluidized bed is also considerably deviant from the fine-grid simulation predictions. In Fig. 8, the instantaneous, as well as mean temperatures of the phases are depicted over the height of the fluidized bed while a mean over the lateral directions was taken. In particular, it can be seen that the overestimation of the bed expansion in the coarse-grid simulation also leads to an underprediction of the temperatures in certain heights of the reactor, since all the inflowing heat is distributed over the overpredicted height of the fluidized bed. In contrast, a SATFM simulation, which incorporates all model corrections to the momentum and energy equations but the drift temperature correction to the interphase heat transfer, i.e. $T_d = 0$, yields better results than the coarse-grid TFM simulation. The difference be-

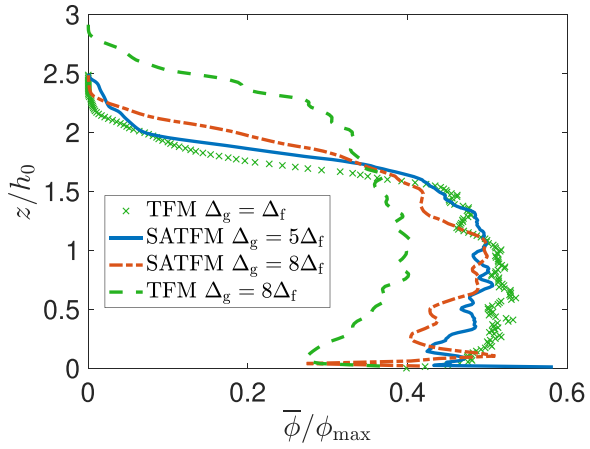

Fig. 7. Predictions for the volume fraction distribution inside the fluidized bed over the height divided by its initial expansion z/h_0. SATFM simulations on two differently coarse grids are compared to TFM simulations on the fine, $\Delta_g = \Delta_f$, and on a coarse, $\Delta_g = 8\Delta_f$, grid.

tween the two test-cases is that the prediction of the volume fraction distribution in the fluidized bed yields a lower mean volume fraction due to the larger bed expansion, while we deliberately kept the volume fraction constant in the periodic domain. Therefore, we conclude that it is essential to have a good prediction for the momentum correction in order to be able to correctly predict the temperature distribution, and furthermore, the reaction rate in real-scale reactors.

In the region close to the inlet, all SATFM simulations yield overestimated values for the temperatures. This is due to the thin nature of the fluidized bed, which forms a region with low solid volume fraction and small clusters of particles just above the inlet, therefore, in the coarse-grid simulations, this area is one big sluggish bubble, where the phase temperatures are high. Even in the fine-grid simulation, this phenomenon can be observed, but it is not as distinct. In the coarse-grid TFM simulation, a bubble seems to have formed in a slightly higher region. In the upper region of the reactor, however, the phase temperatures are correctly estimated by the SATFM for coarse-graining ratios of 5 and 8, where the latter represents 6 grid-cells in the lateral directions. A smaller number of grid-cells was found to not be able to correctly predict the thermo- and hydrodynamics, since it could not properly resolve the larger structures, which is fundamentally necessary for LES models.

The drift temperature correction to the interphase heat transfer seems to have an influence on the mean temperature of the fluidized bed, especially in the upper regions. This would represent the amount of heat that is not immediately transferred to the solid phase where convection and (turbulent) conduction are much lower than in the gas-phase and, therefore, some amount of heat is firstly distributed to the upper regions of the fluidized bed before it is exchanged to the solid phase. A difference between the SATFM

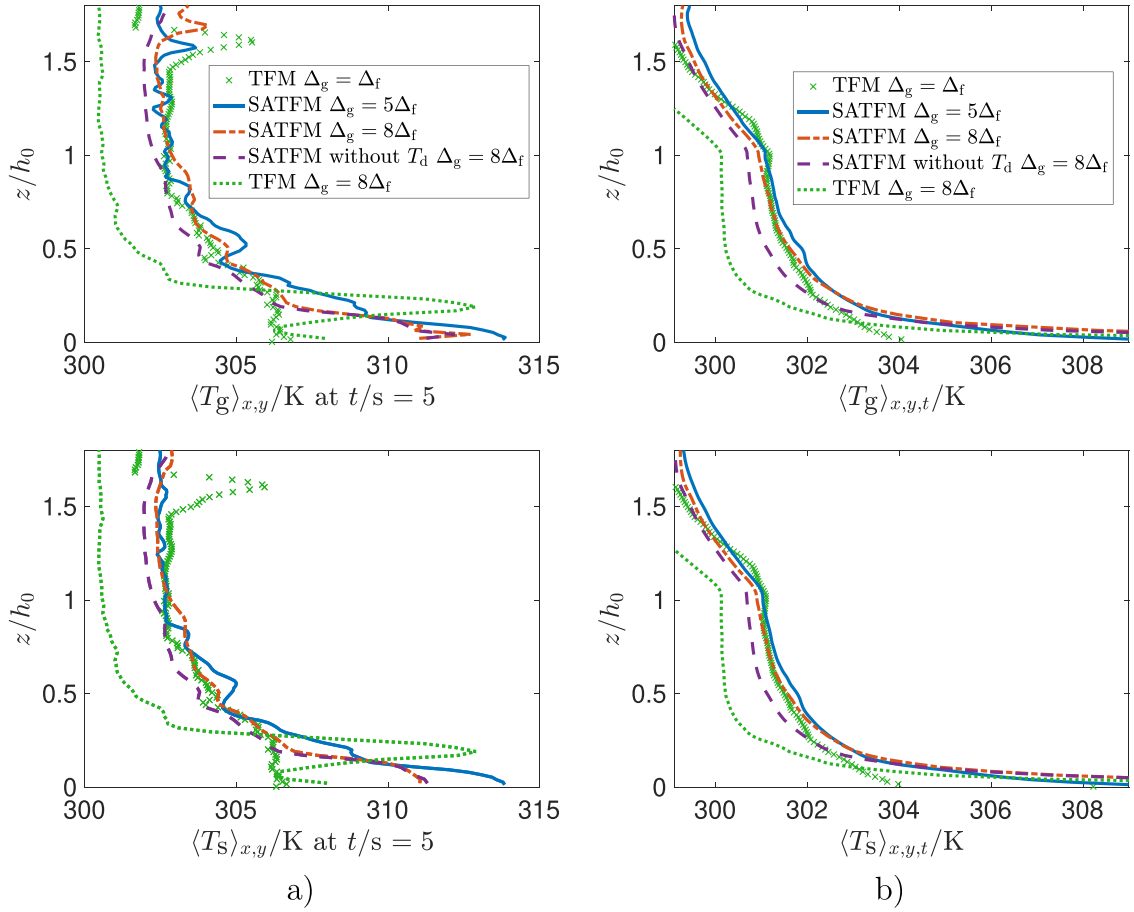

Fig. 8. a) Instantaneous, at $t = 5$ s, and b) mean temperature distributions of the phases in the fluidized bed. We used an average over the lateral components $\langle\rangle_{x,y}$ and depicted the temperature over the height of the fluidized bed divided by its initial height z/h_0. The fine-grid TFM model predictions with $\Delta_g = \Delta_f$ are compared to coarse-grid TFM model simulations with $\Delta_g = 8\Delta_f$ and SATFM model predictions on grids with sizes $\Delta_g = 5\Delta_f$ and $\Delta_g = 8\Delta_f$. Furthermore, a SATFM prediction with $T_d = 0$ is depicted.

predictions with and without the drift temperature correction can especially be observed when the phase temperatures are averaged over time. Therefore, in addition to the heat transfer around local heat sources, which can be produced by reactions, the drift temperature correction seems to play a part in the global temperature distribution, for example during the heat-up of reactors.

Moreover, the correct estimation of the temperature in the upper regions of the fluidized bed depicted in Fig. 8 suggests that, in addition to the drift temperature correction, also the closure models for the other unresolved terms in equations (11) and (12), the dissipation of turbulent kinetic energy and, in particular, the turbulent thermal diffusion, yield valid results. Especially in this set-up, the turbulent conduction plays a role in the distribution of heat from the inlet to the rest of the domain. We want to emphasize that we applied gradient assumption closure models with a turbulent viscosity and turbulent Prandtl number known from single-phase LES modelling for the Reynolds-stress like contributions [1], as stated in Eqs. (11) and (12). As far as we can deduce from Fig. 8, this leads to good predictions for the temperature distributions inside the considered fluidized bed. Although gradient assumptions are generally not as valid in multiphase turbulence modelling [49], we conclude that they yield satisfying results in the considered coarse-grid simulations.

As was already observed in our *a priori* study [1], the viscous dissipation of mean and turbulent kinetic energy does not have a large influence on the overall temperature distribution. In addition, like the *a priori* study [1], this validation case also suggests that the unresolved component of the pressure dilatation, while important for the solution of the turbulent kinetic energy equation of the gas-phase [3], can be neglected in relation to its resolved contribution for the evaluation of the mean temperature.

Finally, we report that the correct prediction of the bed expansion and volume fraction distribution inside the reactor is crucial for the predictions of the heat distribution, as can be deduced from Figs. 7 and 8. Although small deviations, i.e. in slip velocity, still lead to robust predictions, as can be seen in Fig. 3. Furthermore, we conclude that the interphase heat transfer correction by the drift temperature is important for the prediction of the local, as well as, global temperatures of the phases.

5. Conclusions

We validated the SATFM internal energy equation closure models in different set-ups by comparing the predictions on differently coarse grids to fine-grid TFM simulations.

Firstly, we considered unbounded sedimentation of Geldart type A particles with varying domain averaged volume fractions, domain sizes and coarse-graining ratios. After the cluster-induced turbulence was fully developed, we produced an instantaneous temperature difference between the gas- and particle-phase in the whole domain to study the influence of clusters on the interphase heat transfer. This test-case allowed us to isolate and investigate the predictions of the drift temperature correction to the heat transfer. We found that the local, dynamic calculation of the correlation coefficients between the solid volume fraction and the gas-phase temperature leads to good predictions for the drift temperature and, therefore, also for the domain averaged temperature difference decay between the phases. The produced results were valid for a large number of domain averaged solid volume fractions in the moderately dense regime, ranging from 0.05 to 0.25. Additionally, the SATFM model yields satisfying results, which are, to a large degree, independent of the coarse-grid size. This is mainly due to the fact that the sub-grid fluctuating quantities are correctly estimated by the solution of their transport equations using the dynamic approach.

Furthermore, the investigation of a thin cut-out of an elongated fluidized bed reactor of Geldart type B particles showed that the closure models for the other unresolved terms in the thermal energy equation yield good results for the temperature distribution inside the reactor. Especially, a gradient assumption closure model for the turbulent heat flux produces good predictions for the thermal conduction from the fluidized bed's inlet to the higher regions in the reactor.

Finally, we highlight the importance of the correct estimation of the hydrodynamics for the correct prediction of the thermodynamics in moderately dense gas-particle flows and conclude that the SATFM model predictions for the momentum, as well as, for the temperature are promising, even on rather coarse computational grids.

A detailed comparison to full-scale reactor experimental data is still lacking, therefore, a validation study, which also includes corrections to the mass transfer, should be conducted in the future.

Data Availability

Validation study of a Spatially-Averaged Two-Fluid Model for heat transport in gas-particle flows (Mendeley Data).

Declaration of Competing Interest

The authors declare that they have no known competing financial interests or personal relationships that could have appeared to influence the work reported in this paper.

CRediT authorship contribution statement

Stefanie Rauchenzauner: Methodology, Software, Validation, Writing – original draft. **Simon Schneiderbauer:** Conceptualization, Methodology, Software, Writing – review & editing, Supervision.

Acknowledgement

The financial support by the Austrian Federal Ministry for Digital and Economic Affairs and the National Foundation for Research, Technology and Development is gratefully acknowledged. The authors further want to acknowledge the funding support of K1-MET GmbH, metallurgical competence center. The research programme of the K1-MET competence center is supported by COMET (Competence Center for Excellent Technologies), the Austrian programme for competence centers. COMET is funded by the Federal Ministry for Transport, Innovation and Technology, the Federal Ministry for Digital and Economic Affairs and the provinces of Upper Austria, Tyrol and Styria. Beside the public funding from COMET, this research project is partially financed by the industrial partners Primetals Technologies Austria GmbH, voestalpine Stahl Donawitz GmbH, RHI Magnesita GmbH and voestalpine Stahl GmbH.

References

[1] S. Rauchenzauner, S. Schneiderbauer, A dynamic spatially-averaged two-fluid model for heat transport in moderately dense gas-particle flows, Phys. Fluids 32 (2020) 063307.
[2] S. Rauchenzauner, S. Schneiderbauer, A dynamic multiphase turbulence model for coarse-grid simulations of fluidized gas-particle suspensions, Chem. Eng. Sci. 247 (2022) 117104.
[3] S. Rauchenzauner, S. Schneiderbauer, A dynamic anisotropic spatially-averaged two-fluid model for moderately dense gas-particle flows, Int. J. Multiphase Flow 126 (2020) 103237.
[4] S. Schneiderbauer, S. Pirker, Filtered and heterogeneity based subgrid modifications for gas-solid drag and solids stresses in bubbling fluidized beds, AIChE J. 60(3) (2014) 839–854.
[5] R.O. Fox, On multiphase turbulence models for collisional fluid-particle flows, J. Fluid Mech. 742 (2014) 368–424.

[6] S. Sundaresan, A. Ozel, J. Kolehmainen, Toward constitutive models for momentum, species, and energy transport in gas-particle flows, Annu. Rev. Chem. Biomol. Eng. 9 (1) (2018) 61–81.
[7] B. Sun, S. Tenneti, S. Subramaniam, D.L. Koch, Pseudo-turbulent heat flux and average gas-phase conduction during gas-solid heat transfer: flow past random fixed particle assemblies, J. Fluid Mech. 798 (2016) 299–349.
[8] B. Sun, S. Tenneti, S. Subramaniam, Modeling average gas-solid heat transfer using particle-resolved direct numerical simulation, Int. J. Heat Mass Transf. 86 (2015) 898–913.
[9] B. Hou, H. Li, Relationship between flow structure and transfer coefficients in fast fluidized beds, Chem. Eng. J. 157 (2) (2010) 509–519.
[10] K. Agrawal, W. Holloway, C.C. Milioli, F.E. Milioli, S. Sundaresan, Filtered models for scalar transport in gas-particle flows, Chem. Eng. Sci. 95 (2013) 291–300.
[11] Z. Huang, C. Zhang, M. Jiang, Q. Zhou, Development of a filtered interphase heat transfer model based on fine-grid simulations of gas-solid flows, AIChE J. 66 (1) (2020).
[12] Y. Li, Y. Yu, C. Zhang, Z. Huang, Q. Zhou, Improved filtered mesoscale interphase heat transfer model, Particuology 57 (2021) 176–186.
[13] H. Lei, L.-T. Zhu, Z.-H. Luo, Study of filtered interphase heat transfer using highly resolved CFD-DEM simulations, AIChE J. 67 (4) (2021) e17121.
[14] H. Lei, J.-W. Liao, L.-T. Zhu, Z.-H. Luo, CFD-DEM modeling of filtered fluid-particle drag and heat transfer in bidisperse gas-solid flows, Chem. Eng. Sci. 246 (2021) 116896.
[15] L. Lu, A. Morris, T. Li, S. Benyahia, Extension of a coarse grained particle method to simulate heat transfer in fluidized beds, Int. J. Heat Mass Transf. 111 (2017) 723–735.
[16] S. Wang, Y. Shen, Coarse-grained CFD-DEM modelling of dense gas-solid reacting flow, Int. J. Heat Mass Transf. 184 (2022) 122302.
[17] W. Dong, W. Wang, J. Li, A multiscale mass transfer model for gas-solid riser flows: Part II–sub-grid simulation of ozone decomposition, Chem. Eng. Sci. 63 (10) (2008) 2811–2823.
[18] L.-T. Zhu, B. Ouyang, H. Lei, Z.-H. Luo, Conventional and data-driven modeling of filtered drag, heat transfer, and reaction rate in gas-particle flows, AIChE J. 67 (8) (2021) e17299.
[19] S. Beetham, A. Lattanzi, J. Capecelatro, On the thermal entrance length of moderately dense gas-particle flows, Int. J. Heat Mass Trans.f 182 (2022) 121985.
[20] L. Guo, J. Capecelatro, The role of clusters on heat transfer in sedimenting gas–solid flows, Int. J. Heat Mass Transf. 132 (2019) 1217–1230.
[21] O. Simonin, E. Deutsch, J.-P. Minier, Eulerian prediction of the fluid/particle correlated motion in turbulent two-phase flows, Appl. Sci. Res. 51 (1993) 275–283.
[22] A. Ozel, Y. Gu, C.C. Milioli, J. Kolehmainen, S. Sundaresan, Towards filtered drag force model for non-cohesive and cohesive particle-gas flows, Phys. Fluids 29 (October) (2017) 103308.
[23] J.-F. Parmentier, O. Simonin, O. Delsart, A functional subgrid drift velocity model for filtered drag prediction in dense fluidized bed, AIChE J. 58 (4) (2012) 1084–1098.
[24] D. Queteschiner, T. Lichtenegger, S. Schneiderbauer, S. Pirker, Coupling resolved and coarse-grain DEM models, Part. Sci. Technol. 26 (4) (2018) 517–522.
[25] S.B. Pope, Turbulent Flows, Cambridge University Press, Cambridge, UK, 2000.
[26] D.K. Lilly, A proposed modification of the Germano subgrid-scale closure method, Phys. Fluids A 4 (1992) 633–635.
[27] S. Schneiderbauer, A spatially-averaged two-Fluid model for dense large-scale gas-solid flows, AIChE J. 63 (8) (2017) 3544–3562.
[28] C.Y. Wen, Y.H. Yu, Mechanics of fluidization, Chem. Eng. Prog. Symp. Ser. 62 (1966) 100–111.
[29] R. Beetstra, M.A. Van der Hoef, J.A.M. Kuipers, Drag force of intermediate reynolds number flow past mono- and bidisperse arrays of spheres, AIChE J. 53 (2) (2007) 489–501.
[30] C.K.K. Lun, Granular dynamics of inelastic spheres in Couette flow, Phys. Fluids 8 (11) (1996) 2868.
[31] D.L. Koch, Kinetic theory for a monodispers gas-solid suspension, Phys. Fluids A 2 (1990) 1711–1723.
[32] S. Schneiderbauer, S. Puttinger, S. Pirker, Comparative analysis of subgrid drag modifications for dense gas-particle flows in bubbling fluidized beds, AIChE J. 59 (2013) 4077–4099.
[33] D.J. Gunn, Transfer of heat or mass to particles in fixed and fluidised beds, Int. J. Heat Mass Transf. 21 (1978) 467–476.
[34] K. Agrawal, P.N. Loezos, M. Syamlal, S. Sundaresan, The role of meso-scale structures in rapid gas-solid flows, J. Fluid Mech. 445 (2001) 151–185.
[35] M. Germano, Turbulence: the filtering approach, J. Fluid Mech. 238 (1992) 325–336.
[36] S. Schneiderbauer, M. Saeedipour, Numerical simulation of turbulent gas-solid flow using an approximate deconvolution model, Int. J. Multiphase Flow 114 (2019) 287–302.
[37] M. Saeedipour, S. Vincent, S. Pirker, Large eddy simulation of turbulent interfacial flows using approximate deconvolution model, Int. J. Multiphase Flow 112 (2019) 286–299.
[38] P. Sagaut, R. Grohens, Discrete filters for large eddy simulation, Int. J. Numer. Methods Fluids 31 (1999) 1195–1220.
[39] M. Germano, U. Piomelli, P. Moin, W.H. Cabot, A dynamic subgrid-scale eddy viscosity model, Phys. Fluids A 3 (1991) 1760–1765.
[40] W.D. Fullmer, C.M. Hrenya, Quantitative assessment of fine-grid kinetic-theory-based predictions of mean-slip in unbounded fluidization, AIChE J. 61 (1) (2016) 11–17.
[41] C. Guenther, M. Syamlal, The effect of numerical diffusion on simulation of isolated bubbles in a gas-solid fluidized bed, Powder Tech. 116 (2) (2001) 142–154.
[42] Y. Liu, O. Hinrichsen, CFD modeling of bubbling fluidized beds using OpenFOAMë: model validation and comparison of TVD differencing schemes, Comp. Chem. Eng. 69 (2014) 75–88.
[43] D.G. Schaeffer, Instability in the evolution equations describing incompressible granular flow, J. Differ. Equ. 66 (1987) 19–50.
[44] S. Schneiderbauer, A. Aigner, S. Pirker, A comprehensive frictional-kinetic model for gas-particle flows: analysis of fluidized and moving bed regimes, Chem. Eng. Sci. 80 (2012) 279–292.
[45] S. Radl, S. Sundaresan, A drag model for filtered Euler-Lagrange simulations of clustered gas-particle suspensions, Chem. Eng. Sci. 117 (2014) 416–425.
[46] W.D. Fullmer, G. Liu, X. Yin, C.M. Hrenya, Clustering instabilities in sedimenting fluid-solid systems: critical assessment of kinetic-theory-based predictions using direct numerical simulation data, J. Fluid Mech. 823 (2017) 433–469.
[47] S. Schneiderbauer, M. Saeedipour, Sub-grid deconvolution approach for filtered two-fluid models and the application to fluidized gas-particle suspensions, in: M. Deville, C. Calvin, V. Couaillier, M. De La Llave Plata, J.-L. Estivalèzes, T.H. Lê, S. Vincent (Eds.), Turbulence and Interactions (TI 2018). Notes on Numerical Fluid Mechanics and Multidisciplinary Design, vol. 149, Springer Nature Switzerland AG, Les Trois-Îlets, Martinique, France, 2021, pp. 183–188.
[48] S. Balachandar, M. Ha, A note on thermal history kernel for unsteady heat transfer of a spherical particle, Int. J. Heat Mass Transf. 180 (2021) 121781.
[49] F. Dabbagh, S. Schneiderbauer, Small-scale flow topologies, pseudo-turbulence, and impact on filtered drag models in turbulent fluidization, Phys. Rev. Fluids 6 (2021) 074301.